NOTES

Chemotaxis to the Quorum-Sensing Signal AI-2 Requires the Tsr Chemoreceptor and the Periplasmic LsrB AI-2-Binding Protein[▽]

Manjunath Hegde,[1]† Derek L. Englert,[1]† Shanna Schrock,[1] William B. Cohn,[2] Christian Vogt,[2]‡ Thomas K. Wood,[1] Michael D. Manson,[2]* and Arul Jayaraman[1]*

Department of Chemical Engineering[1] and Department of Biology,[2] Texas A&M University, College Station, Texas

AI-2 is an autoinducer made by many bacteria. LsrB binds AI-2 in the periplasm, and Tsr is the L-serine chemoreceptor. We show that AI-2 strongly attracts *Escherichia coli*. Both LsrB and Tsr are necessary for sensing AI-2, but AI-2 uptake is not, suggesting that LsrB and Tsr interact directly in the periplasm.

Many functions in bacteria are regulated by population density, including formation of biofilms and production of virulence factors (5). Assessment of population density, known as quorum sensing, relies on the ability of cells to determine the concentrations of compounds known as autoinducers (AIs). As the cell density increases, an AI accumulates to a concentration that triggers a quorum-sensing response. Autoinducers activate some genes and repress others. Induced genes typically include those responsible for production of the autoinducer, resulting in a positive feedback loop. Cell densities required to accumulate enough AI for good induction are 10^8 per ml or higher.

AIs are of two basic types: species specific and general (22). Species-specific AI-1s are acyl homoserine lactones in Gram-negative bacteria and modified peptides in Gram-positive bacteria. Full induction of bioluminescence in the marine bacterium *Vibrio harveyi*, which colonizes dead organic matter, requires both a specific AI-1 inducer and a general autoinducer, called AI-2 (6). AI-2 is derived from spontaneous cyclization of 4,5-dihydroxy-2,3-pentanedione (DPD). DPD is made from *S*-ribosylhomocysteine by the enzyme LuxS (25). *S*-Ribosylhomocysteine is an intermediate in the breakdown of *S*-adenosylhomocysteine, the product remaining after methyl group donation by *S*-adenosylmethionine.

AI-2 is produced by a wide range of Gram-negative and Gram-positive bacteria and exists in multiple forms that are in equilibrium with each other (5). The form that is active in *V. harveyi* is (2*S*,4*S*)-2-methyl-2,3,3,4-tetrahydroxytetrahydrofuran borate (S-THMF borate) (8), which binds to the periplasmic protein LuxP. In *S. enterica* serovar Typhi-

murium, a boron-free isomer of AI-2 [(2*R*,4*S*)-2-methyl-2,3,3,4-tetrahydroxytetra-hydrofuran (R-THMF)] binds to the periplasmic LsrB protein (21). LsrB is the recognition component of an ABC transporter for AI-2. LsrACD are the membrane-bound components of the ABC transporter for AI-2. AI-2 is generated by the enzyme LuxS, and the YdgG (TqsA) protein has been implicated in AI-2 export from the cytoplasm (14).

AI-2 is a known chemoattractant for *Escherichia coli* (4, 10), but the receptor(s) involved in AI-2 sensing has not been identified. This work was initiated to characterize the proteins involved in AI-2 recognition by *E. coli* strain CV1, which is equivalent to the standard wild-type chemotaxis strain RP437. The strains used in this study are shown in Table 1.

The microplug (μPlug) assay (9), a modified plug-in-pond assay, provides a qualitative but highly visual representation of chemotaxis. Cells containing the green fluorescent protein (GFP)-encoding plasmid pCM18 were grown overnight at 32°C in tryptone broth (TB) (20) containing 150 μg/ml erythromycin. Cells were back-diluted to a turbidity of 0.05 at 600 nm in 25 ml of TB lacking erythromycin and then grown to mid-logarithmic phase (turbidity of 0.5 at 600 nm) at 32°C. Cells were examined by phase-contrast microscopy to ensure robust motility and normal run-tumble swimming behavior. The cells were harvested by low-speed centrifugation at 400 × *g* for 5 min, gently washed twice with chemotaxis buffer (CB; phosphate-buffered saline, 0.1 mM EDTA, 0.01 mM L-methionine, and 10 mM D,L-lactate) and then gently resuspended in 2 ml of CB. These cells were again examined under the microscope to ensure robust motility and normal run-tumble swimming behavior. Cells were mixed with an approximately equal number of TG1 cells expressing red fluorescent protein (RFP) from plasmid pDS-Red Express that had been killed by a 1-h treatment with 1 mg/ml kanamycin. The dead RFP-containing cells served as a control to visualize any mixing due to turbulence within the microfluidic chamber.

The responses of *E. coli* strain CV1 and its isogenic *tsr* and *lsrB* mutant derivatives are shown in Fig. 1. In the absence of AI-2 in the plug, CV1 cells distributed themselves randomly (Fig. 1A). However, when CV1 cells were exposed to plugs

---

* Corresponding author. Mailing address for A. Jayaraman: 3122 TAMU, Texas A&M University, College Station, TX 77843-3122. Phone: (979) 845-3306. Fax: (979) 845-6446. E-mail: arulj@tamu.edu. Mailing address for M. D. Manson: 3258 TAMU, Texas A&M University, College Station, TX 77843-3258. Phone: (979) 845-5158. Fax: (979) 845-2891. E-mail: mike@mail.bio.tamu.edu.

† M. Hegde and D. L. Englert were equal contributors.

‡ Present address: Novartis Pharma AG, PharmOps CH QA/Biological and Microbiological Services, Stein CH-4332, Switzerland.

▽ Published ahead of print on 19 November 2010.

TABLE 1. Bacterial strains and plasmids

Strain or plasmid	Genotype	Resistance[a]	Source
Escherichia coli strains			
CV1	Chemotaxis wild type (same as RP437)	Str	24
TG1/pDS-Red Express	Wild type; dead-cell control	Amp	Stratagene
CV5	CV1 Δ*tsr*	Str	This study[b]
CV12	CV1 Δ*tar-tap trg*::Tn*10*	Str, Tet	This study[c]
MJ101	CV1 *lsrB*ΩKan[r]	Str, Kan	This study[d]
MJ102	CV1 *lsrC*ΩKan[r]	Str, Kan	This study[e]
BW25113 Δ*lsrB*	*lsrB*ΩKan[r]	Kan	3
BW25113 Δ*lsrC*	*lsrC*ΩKan[r]	Kan	3
Plasmids			
pCM18	GFP-expressing vector	Erm	12
pDS-RedExpress	RFP-expressing vector	Amp	Clontech
pCA24N-*lsrB*	pCA24N P_{T5-lac}::*lsrB*; expresses *E. coli* *lsrB* from p*lacZYA*	Cm	15

[a] Str, streptomycin; Tet, tetracycline; Kan, kanamycin; Erm, erythromycin; Amp, ampicillin; Cm, chloramphenicol.
[b] Made by introducing Δ*tsr9101* (7) into CV1 by phage P1 transduction (16), with selection for Thr[+] and screening for Tsr[−].
[c] Made in two steps: Δ*tar-tap5201* (26) was introduced into CV1 by phage P1 transduction with selection for Eda[+], followed by screening for Tar[−], and then *trg*::Tn*10* was introduced by phage P1 transduction followed by selection for Tet[r] on lysis broth (LB) (20) agar plates containing 10 μg/ml tetracycline, followed by screening for Trg[−].
[d] Made by introducing *lsrB*ΩKan[r] (3) into CV1 by phage P1 transduction, with selection for Kan[r] and confirmation of *lsrB* gene disruption by PCR.
[e] Made by introducing *lsrC*ΩKan[r] (3) into CV1 by phage P1 transduction, with selection for Kan[r] and confirmation of *lsrC* gene disruption by PCR.

containing 200 μM L-serine or 200 μM AI-2, they exhibited strong attractant responses, shown by the accumulation of bacteria at the agarose plug-liquid interface (Fig. 1B and C). Strain CV5 (CV1 Δ*tsr*), which lacks the L-serine receptor Tsr, did not respond to L-serine (Fig. 1D) and gave a severely attenuated response to AI-2 (Fig. 1E). Strain CV12 (CV1 Δ*tar-tap* Δ*trg*), which has Tsr as its only functional receptor (other than Aer), responded to both L-serine and AI-2 (data not shown), although the accumulation was somewhat decreased relative to that of strain CV1. Thus, Tsr is both necessary and sufficient for good AI-2 chemotaxis in *E. coli* K-12, although there may be a small residual response in cells lacking Tsr.

Because AI-2 is known to bind to the periplasmic protein LsrB, we also looked at the responses of MJ101 (CV1 *lsrB*ΩKan[r]) cells. These cells responded like strain CV1 to L-serine (Fig. 1F) but showed no accumulation around plugs containing 200 μM AI-2 (Fig. 1G). In contrast, MJ102 (CV1 *lsrC*ΩKan[r]) cells, which should still produce LsrB but not be able to take up AI-2 into the cytoplasm, accumulated around plugs containing 200 μM L-serine (data not shown) or 200 μM AI-2 (Fig. 1H). The accumulation near AI-2 plugs was somewhat weaker than that of strain CV1, perhaps because of a polar effect of the *lsrC*ΩKan[r] insertion on the downstream *lsrB* gene in the *lsrACDBFGE* operon (28). MJ101 cells containing
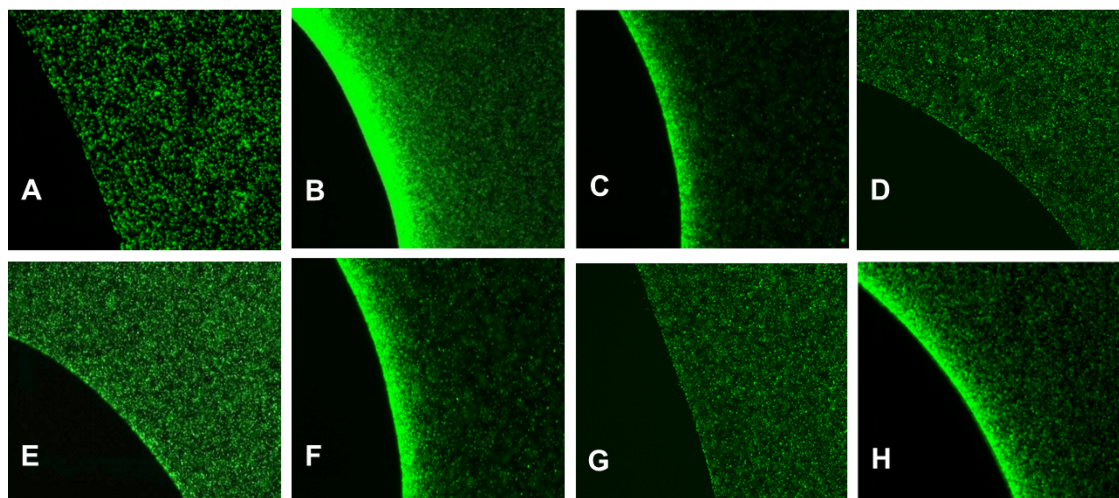

FIG. 1. Chemotactic responses to L-serine and AI-2, demonstrated by the results of μPlug assays. The μPlug assay was carried out as described in the text and as previously reported (10, 19); the distribution of dead, RFP-labeled cells is not shown, but it was always uniform except when the dead cells were displaced around the plug by accumulating GFP-labeled motile cells. (A) Distribution of wild-type (CV1) cells in the absence of any attractant in the plug. (B) Distribution of wild-type (CV1) cells with 200 μM L-serine in the plug. (C) Distribution of wild-type (CV1) cells with 200 μM AI-2 in the plug. (D) Distribution of Δ*tsr* (CV5) cells with 200 μM L-serine in the plug. (E) Distribution of Δ*tsr* (CV5) cells with 200 μM AI-2 in the plug. (F) Distribution of *lsrB*ΩKan[r] (MJ101) cells with 200 μM L-serine in the plug. (G) Distribution of *lsrB*ΩKan[r] (MJ101) cells with 200 μM AI-2 in the plug. (H) Distribution of *lsrC*ΩKan[r] (MJ102) cells with 200 μM AI-2 in the plug.
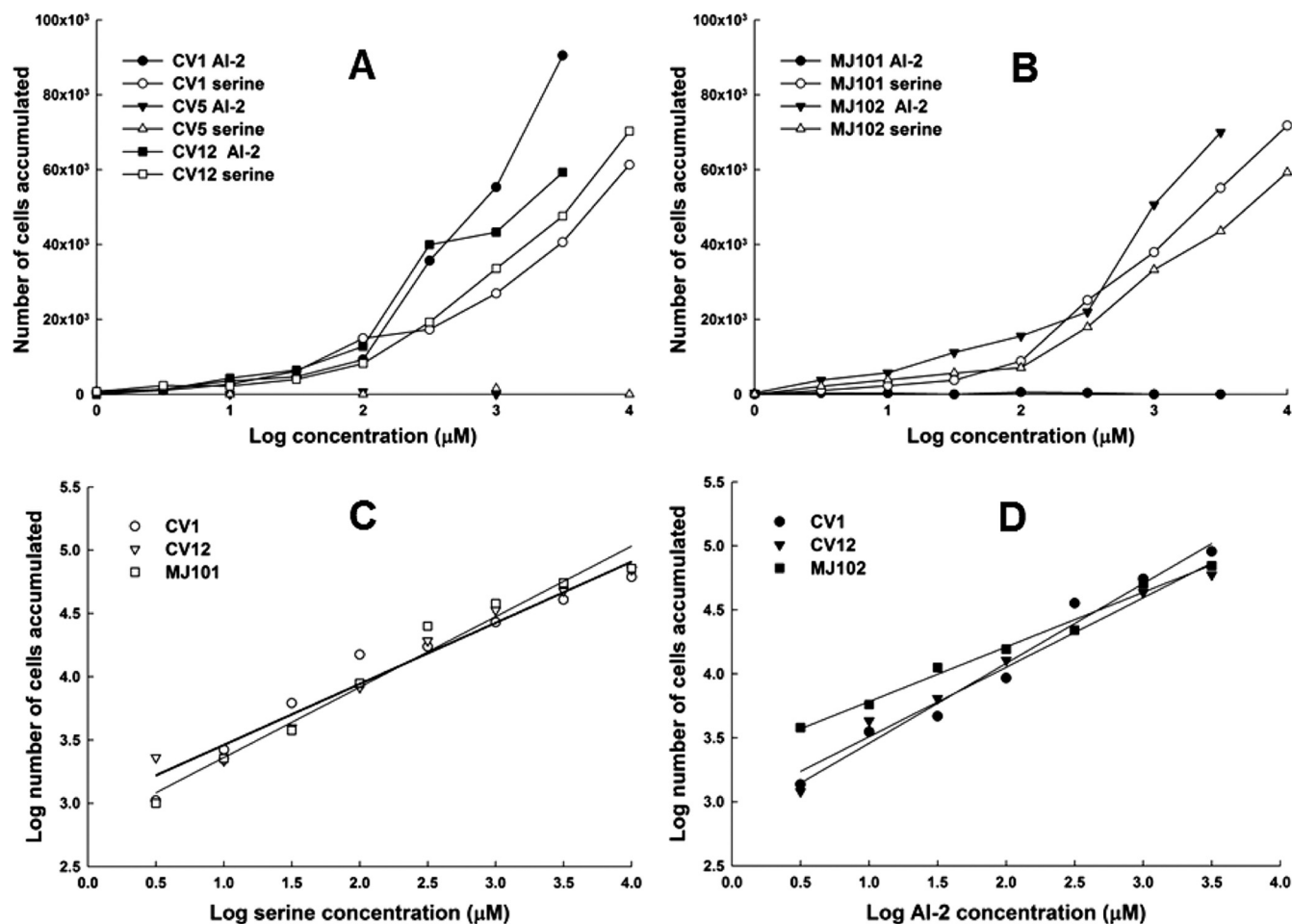
FIG. 2. Responses of cells to L-serine and AI-2 in the capillary assay. Assays were performed at 32°C, essentially as described by Adler (1). Cells were resuspended in CB to a cell density of about 5×10^7/ml. Assays were run twice, with three capillaries per run for each strain under each condition. Data shown are averages of six capillaries, and the standard deviations (not shown for purposes of clarity) ranged from 10 to 20%. The background accumulations in buffer-only capillaries were in the range of 500 to 1,000 cells. (A) Normalized values (with buffer-only control subtracted) of CV1 (wild-type) cells, CV5 (Δtsr) cells, and CV12 (Δtar-tap Δtrg) cells exposed to capillaries containing L-serine or AI-2. (B) Normalized values of MJ101 ($lsrB\Omega$Kan^r) cells and MJ102 ($lsrC\Omega$Kan^r) cells exposed to capillaries containing L-serine or AI-2. (C) Data for the responses of CV1, CV12, and MJ101 cells to L-serine, plotted on a log-log scale. The straight lines are linear regressions that can be extrapolated back to a threshold value. The extrapolated threshold concentrations, as predicted by Weber's law, are 1.7×10^{-12} M for strain CV12 and 3.5×10^{-12} M for strains CV1 and MJ101. The regression lines for CV12 and MJ101 were identical. (D) Data for the responses of CV1, CV12, and MJ102 cells to AI-2, plotted on a log-log scale. The linear regressions can be extrapolated back to a threshold value. The extrapolated threshold concentrations are 1.6×10^{-11} for strain CV1, 4.6×10^{-12} M for strain CV12, and 2.5×10^{-14} M for strain MJ102.

plasmid pCA24N-$P_{T5\text{-}lac}$::$lsrB$, which encodes wild-type E. coli LsrB, accumulated around AI-2-containing plugs about as well as MJ102 cells (data not shown) when 1 mM isopropyl β-D-1-thiogalactopyranoside (IPTG) was added to induce LsrB synthesis.

To quantify the response to AI-2 and to compare it to the response to L-serine, we performed capillary assays (1). As expected from the μPlug assay results, CV1 and CV12 cells accumulated in capillaries containing either L-serine or AI-2 (Fig. 2A), with the CV1 strain giving a stronger response, whereas CV5 (Δtsr) cells did not accumulate in capillaries containing either compound. MJ101 cells ($lsrB\Omega$Kan^r) responded to L-serine but not to AI-2, whereas MJ102 cells ($lsrC\Omega$Kan^r) responded to both (Fig. 2B). Thus, the conclusions from the μPlug assay were confirmed.

By plotting the data from the capillary assay on a log-log

plot, we could extrapolate a threshold concentration for both compounds in each strain (19). With L-serine, the extrapolated detection thresholds for strains CV1, CV12, and MJ101 were all in the range of 2×10^{-12} to 4×10^{-12} M (Fig. 2C). The result was quite different with AI-2, because strains CV1 and CV12 had extrapolated detection thresholds of $\sim 5 \times 10^{-12}$ and 2×10^{-11} M, respectively, but the extrapolated detection threshold for the LsrC$^-$ strain MJ102 was at least 100-fold lower, $\sim 2 \times 10^{-14}$ M (Fig. 2D). This is the expected result if the periplasmic AI-2 concentration in MJ102 cells is higher than in CV1 cells, because in the latter strain AI-2 is cleared from the periplasm by transport into the cell. The same phenomenon has been seen with cells containing maltose-binding protein in the absence of a functional maltose transport system (29).

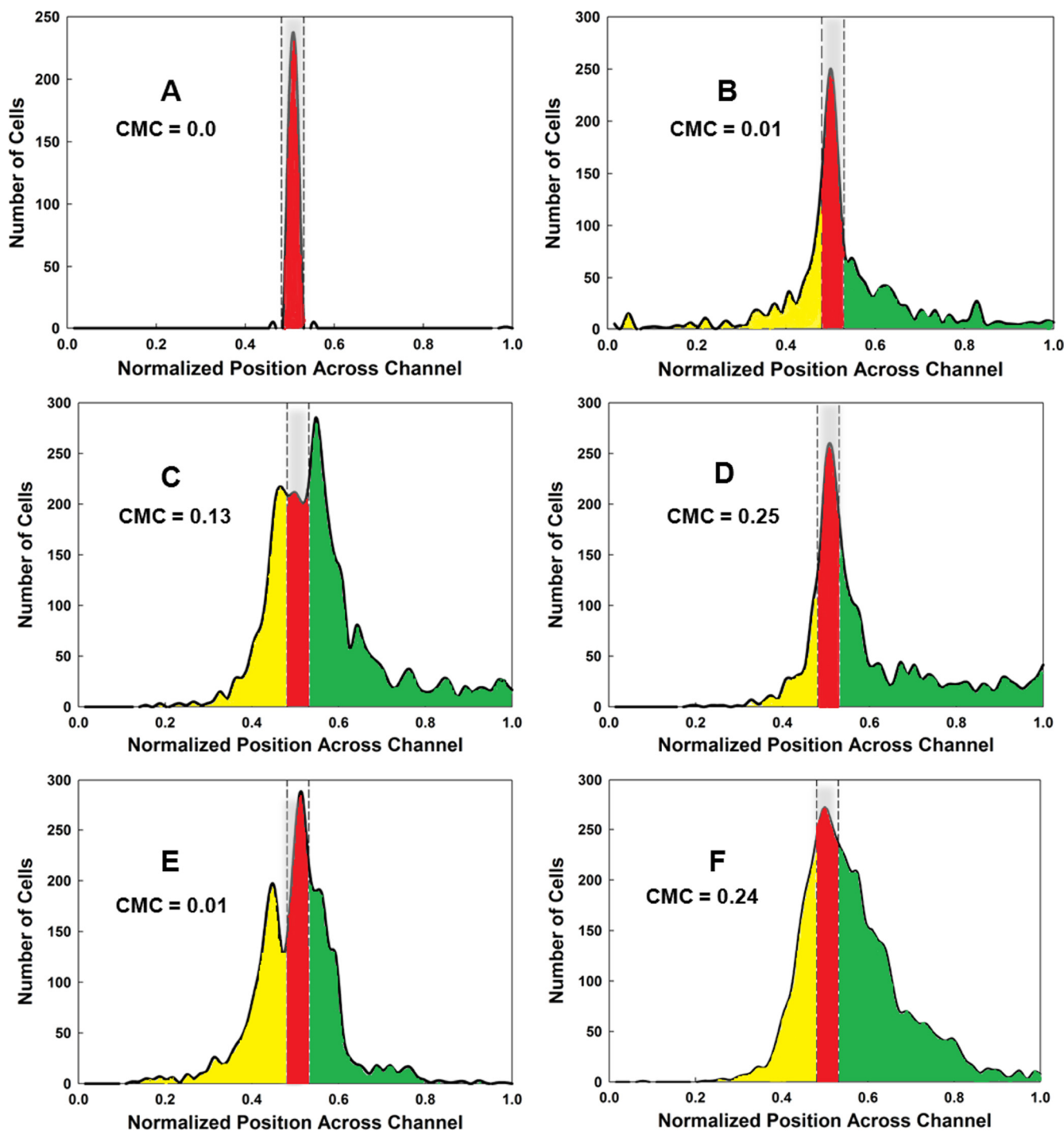To test the relative sensitivity of cells to L-serine and AI-2 in

FIG. 3. Assays of chemotactic behavior in the μFlow device. Cells were grown and prepared as for the μPlug assay, as described previously (9). The CMC was calculated according to the methods described in the text and elsewhere (10, 18). (A) Typical distribution of RFP-labeled dead cells, shown in red. The distribution of cells from one run is shown; it is typical for that found for RFP-labeled dead cells in all runs. The area occupied by dead cells is delineated by the gray bar enclosed in dashed lines. (B) Typical distribution of CV1 (wild-type) GFP-labeled cells in the absence of a chemoeffector gradient. The distribution of cells moving in the up-gradient direction beyond the "dead" zone is highlighted in green, and the distribution of cells moving in the down-gradient direction is highlighted in yellow. GFP-labeled cells remaining in the region occupied by dead cells (highlighted in red) were not included in the calculations of CMC values. (C) Typical distribution of CV1 cells in a 0-to-200 μM nonlinear gradient of L-serine. (D) Typical distribution of CV1 cells in a 0-to-200 μM nonlinear gradient of AI-2. (E) Typical distribution of CV1 cells in a 0-to-200 μM linear gradient of L-serine. (F) Typical distribution of CV1 cells in a 0-to-200 μM linear gradient of L-serine. All assays were run a minimum of three times. The CMC values obtained are indicated on each graph.

an independent assay, we employed the µFlow device (9, 10). The gradients were created in two ways. In the first scenario, a linear gradient was generated across the 1,050-µm width of the microfluidic observation chamber by utilizing two input channels, delivering 0 and 200 µM chemoeffector. In the second scenario, a nonlinear gradient was generated by using five input channels to deliver 0, 0, 2, 20, and 200 µM chemoeffector. The concentration at the entry point for the cells was 100 µM in the linear gradient and 2 µM in the nonlinear gradient, and the cells were preequilibrated with these concentrations prior to their introduction into the observation chamber. The distribution profiles of fluorescently labeled CV1 cells in L-serine and AI-2 are shown in Fig. 3. For each set of conditions, the chemotaxis migration coefficients (CMC values) (10, 18) were calculated (Fig. 3). Basically, the CMC value represents the difference in the total number of cells migrating in the up-gradient direction minus the total number of cells migrating in the down-gradient direction, with the cell values weighted by the fractional distance they moved toward a boundary. Thus, cells migrating all the way to the right or left walls of the chamber received a weighting factor of 1 or -1, respectively, cells migrating halfway to the right or left walls received weighting factors of 0.5 or -0.5, and so forth.

CV1 cells responded to nonlinear and linear gradients of AI-2 (Fig. 3D and F) with similar CMC values (0.24 and 0.25), but they responded significantly only to the nonlinear gradient of L-serine, in which the gradient is very steep at the point at which the cells enter the chamber (compare Fig. 3C and E). Even in the nonlinear gradient, the CMC value for L-serine was only 0.13, about 50% that of the CMC value for AI-2. These results are consistent with the idea that chemotaxis to AI-2 is more sensitive at higher chemoeffector concentrations than is chemotaxis to L-serine.

We also tested the MJ102/pCA24N-$P_{T5\text{-}lac}$::*lsrB* strain in a nonlinear AI-2 gradient in the µFlow device. It gave a CMC value of 0.18, which was lower than the value for CV1 cells in nonlinear AI-2 gradients but higher than that for CV1 cells in nonlinear gradients of L-serine. At present, we have no way of measuring periplasmic levels of LsrB, but the somewhat-attenuated response of MJ102/pCA24N-$P_{T5\text{-}lac}$::*lsrB* cells relative to wild-type cells could reflect nonphysiological levels of LsrB in the complemented strain.

Preliminary evidence from µPlug assays (M. Hegde, unpublished data) suggests that the pathogenic *S.* Typhimurium strain 14028 also responds to AI-2 as an attractant and uses Tsr and LsrB to mediate that response. It may well be that many motile bacteria that produce the Tsr and LsrB proteins share the ability to perform chemotaxis to AI-2.

The reason why LsrB is essential for chemotaxis to AI-2 is not known. The role of LsrB in chemotaxis does not seem to be for transport of AI-2 into the cytoplasm, because strain MJ102, which carries the *lsrC*ΩKan^r mutation, is defective for AI-2 transport (27) but is still able to carry out AI-2 chemotaxis. By analogy with other binding protein-dependent chemoreceptor systems, such as those for maltose-binding protein (MBP) and Tar (29), it may be that AI-2-bound LsrB assumes a conformation that enables it to interact with Tsr directly in the periplasm. Similar interactions have been postulated for the involvement of galactose-binding protein (13) and ribose-binding protein (2) with Trg in taxis to these two sugars and for

dipeptide-binding protein with Tap (17). Tsr is the only one of the four canonical chemoreceptors of *E. coli* not known to interact with a substrate-binding protein. It may be on the verge of losing that unique status.

The typical paradigm for indirectly binding chemoreceptors is that the ligands have a micromolar K_D (equilibrium dissociation constant) for the periplasmic binding protein, and the ligand-bound binding protein has a low affinity for its chemoreceptor partner, estimated at about 200 µM for MBP and Tar (29). The K_D for AI-2 binding to LsrB has been reported as $\sim$160 µM (30), which is at least 100-fold higher than the K_D of MBP for maltose. We do not know the levels of LsrB in the periplasm of cells grown under various conditions, but they may be significantly lower than for other binding proteins, which typically far outnumber their cognate membrane-bound transport systems and chemoreceptors. Thus, the binding affinities of AI-2 for LsrB and of AI-2-bound LsrB for Tsr could be very different than for other known indirectly binding chemoreceptors.

AI-2, unlike other known attractants for *E. coli*, does not serve as food for bacteria (28) but is an intraspecific and interspecific signal of cell density. Therefore, chemotaxis to AI-2 may not have the rather narrow dose-response range that is characteristic of most indirectly binding chemoattractants (23). For nutrients, migration to concentrations higher than those needed for the maximum rate of uptake has no selective value. Given that AI-2 is produced by many different species of biofilm-forming bacteria (5), it may be that chemotaxis to AI-2 serves to recruit free-swimming, planktonic bacteria to biofilms (11). If so, there is no obvious reason why the response to AI-2 should saturate; the selective pressure may be to swim as close as possible to a source of AI-2. We are currently characterizing the molecular mechanism of AI-2 chemotaxis in order to understand how it has evolved to match the ecological context in which AI-2 chemotaxis occurs.

REFERENCES

1. **Adler, J.** 1973. A method for measuring chemotaxis and use of the method to determine optimum conditions for chemotaxis by *Escherichia coli*. J. Gen. Microbiol. **74:**77–91.
2. **Aksamit, R. R., and D. E. Koshland, Jr.** 1974. Identification of the ribose binding protein as the receptor for ribose chemotaxis in *Salmonella typhimurium*. Biochemistry **13:**4473–4478.
3. **Baba, T., et al.** 2006. Construction of *Escherichia coli* K-12 in-frame, single-gene knockout mutants: the Keio collection. Mol. Syst. Biol. **2:**2006–2008.
4. **Bansal, T., P. Jesudhasan, S. Pillai, T. K. Wood, and A. Jayaraman.** 2008. Temporal regulation of enterohemorrhagic *Escherichia coli* virulence mediated by autoinducer-2. Appl. Microbiol. Biotechnol. **78:**811–819.
5. **Bassler, B. L.** 2002. Small talk: cell-to-cell communication in bacteria. Cell **109:**421–424.
6. **Bassler, B. L., M. Wright, and M. R. Silverman.** 1994. Multiple signalling systems controlling expression of luminescence in *Vibrio harveyi*: sequence and function of genes encoding a second sensory pathway. Mol. Microbiol. **13:**273–286.
7. **Callahan, A. M., and J. S. Parkinson.** 1985. Genetics of methyl-accepting chemotaxis proteins in *Escherichia coli*: *cheD* mutations affect the structure and function of the Tsr transducer. J. Bacteriol. **161:**96–104.

8. **Chen, X., et al.** 2002. Structural identification of a bacterial quorum-sensing signal containing boron. Nature **415:**545–549.

9. **Englert, D. L., A. Jayaraman, and M. D. Manson.** 2009. Microfluidic techniques for the analysis of bacterial chemotaxis. Methods Mol. Biol. **571:**1–23.

10. **Englert, D. L., M. D. Manson, and A. Jayaraman.** 2009. Flow-based microfluidic device for quantifying bacterial chemotaxis in stable, competing gradients. Appl. Environ. Microbiol. **75:**4557–4564.

11. **Gonzalez Barrios, A. F., et al.** 2006. Autoinducer 2 controls biofilm formation in *Escherichia coli* through a novel motility quorum-sensing regulator (MqsR, B3022). J. Bacteriol. **188:**305–316.

12. **Hansen, M. C., R. J. Palmer, Jr., C. Udsen, D. C. White, and S. Molin.** 2001. Assessment of GFP fluorescence in cells of *Streptococcus gordonii* under conditions of low pH and low oxygen concentration. Microbiology **147:**1383–1391.

13. **Hazelbauer, G. L., and J. Adler.** 1971. Role of the galactose binding protein in chemotaxis of *Escherichia coli* toward galactose. Nat. New Biol. **230:**101–104.

14. **Herzberg, M., I. K. Kaye, W. Peti, and T. K. Wood.** 2006. YdgG (TqsA) controls biofilm formation in *Escherichia coli* K-12 through autoinducer 2 transport. J. Bacteriol. **188:**587–598.

15. **Kitagawa, M., et al.** 2005. Complete set of ORF clones of *Escherichia coli* ASKA library (a complete set of E. coli K-12 ORF archive): unique resources for biological research. DNA Res. **12:**291–299.

16. **Maeda, T., V. Sanchez-Torres, and T. K. Wood.** 2008. Metabolic engineering to enhance bacterial hydrogen production. Microb. Biotechnol. **1:**30–39.

17. **Manson, M. D., V. Blank, G. Brade, and C. F. Higgins.** 1986. Peptide chemotaxis in *E. coli* involves the Tap signal transducer and the dipeptide permease. Nature **321:**253–256.

18. **Mao, H., P. S. Cremer, and M. D. Manson.** 2003. A sensitive, versatile microfluidic assay for bacterial chemotaxis. Proc. Natl. Acad. Sci. U. S. A. **100:**5449–5454.

19. **Mesibov, R., G. W. Ordal, and J. Adler.** 1973. The range of attractant concentrations for bacterial chemotaxis and the threshold and size of response over this range. Weber law and related phenomena. J. Gen. Physiol. **62:**203–223.

20. **Miller, J. H.** 1972. Experiments in molecular genetics. Cold Spring Harbor Laboratory, Cold Spring Harbor, NY.

21. **Miller, S. T., et al.** 2004. *Salmonella typhimurium* recognizes a chemically distinct form of the bacterial quorum-sensing signal AI-2. Mol. Cell **15:**677–687.

22. **Mok, K. C., N. S. Wingreen, and B. L. Bassler.** 2003. *Vibrio harveyi* quorum sensing: a coincidence detector for two autoinducers controls gene expression. EMBO J. **22:**870–881.

23. **Neumann, S., C. H. Hansen, N. S. Wingreen, and V. Sourjik.** 2010. Differences in signalling by directly and indirectly binding ligands in bacterial chemotaxis. EMBO J. **29:**3484–3495.

24. **Parkinson, J. S., and S. E. Houts.** 1982. Isolation and behavior of *Escherichia coli* deletion mutants lacking chemotaxis functions. J. Bacteriol. **151:**106–113.

25. **Schauder, S., K. Shokat, M. G. Surette, and B. L. Bassler.** 2001. The LuxS family of bacterial autoinducers: biosynthesis of a novel quorum-sensing signal molecule. Mol. Microbiol. **41:**463–476.

26. **Slocum, M. K., and J. S. Parkinson.** 1983. Genetics of methyl-accepting chemotaxis proteins in *Escherichia coli*: organization of the *tar* region. J. Bacteriol. **155:**565–577.

27. **Taga, M. E., S. T. Miller, and B. L. Bassler.** 2003. Lsr-mediated transport and processing of AI-2 in *Salmonella typhimurium*. Mol. Microbiol. **50:**1411–1427.

28. **Taga, M. E., J. L. Semmelhack, and B. L. Bassler.** 2001. The LuxS-dependent autoinducer AI-2 controls the expression of an ABC transporter that functions in AI-2 uptake in *Salmonella typhimurium*. Mol. Microbiol. **42:**777–793.

29. **Zhang, Y., et al.** 1999. Model of maltose-binding protein/chemoreceptor complex supports intrasubunit signaling mechanism. Proc. Natl. Acad. Sci. U. S. A. **96:**939–944.

30. **Zhu, J., and D. Pei.** 2008. A LuxP-based fluorescent sensor for bacterial autoinducer II. ACS Chem. Biol. **3:**110–119.